Supporting Information

Effect of Nanoscale Confinement on the Crystallization of Potassium Ferrocyanide

Clara Anduix-Canto[1], Yi-Yeoun Kim[1], Yunwei Wang[1], Alex N. Kulak[1], Fiona C. Meldrum[1†] and Hugo K. Christenson[2*]

[1]School of Chemistry, University of Leeds, Woodhouse Lane, Leeds, LS2 9JT, UK.

[2]School of Physics and Astronomy, University of Leeds, Leeds, LS2 9JT, UK.

*corresponding author: e-mail: h.k.christenson@leeds.ac.uk

† corresponding author: e-mail: f.meldrum@leeds.ac.uk

Analysis of Electron Diffraction Patterns

The indexing of the diffraction patterns of the rectangular and octagonal crystals is summarized in Table S1, showing reflections of the (103), (422) and (32-1) planes where the measured distances between planes were d(103) = 2.90 Å, d(422) = 2.06 Å and d(32-1) = 2.84 Å and the measured angles between the planes were θ(103/32-1) = 90.3°, θ(103/422) = 46.9° and θ(422/32-1) = 43.7°. The planes observed in the diffraction pattern of an octagonal crystal were (11-3), (311) and (42-2) and the measured distances between planes were d(11-3) = 2.93 Å, d(311) = 2.90 Å and d(42-2) = 2.01 Å, and the angles between the planes were θ(11-3/311) = 88.0°, θ(11-3/42-2) = 43.9° and θ(311/42-2) = 43.7°. In the case of the hexagonal crystals we could observe reflections of the planes (104), (214) and (110) with measured distances between the planes of d(104) = 6.25 Å, d(214) = 3.72 Å and d(110) = 6.58 Å and the angles between the planes were θ(104/214) = 30.1°, θ(214/110) = 30.6° and θ(110/104) = 61.1°.

Crystal shape	Crystal system	Plane	Calculate d(Å)	d(Å) sample	Angles between planes	Measured angles (°)	Calculated angles (°)
Rectangular	Monoclinic C2/c	(103)	2.97	2.90	θ(103/32-1)	90.3	90.0
		(422)	2.04	2.06	θ(103/422)	46.9	46.7
		(32-1)	2.93	2.84	θ(422/32-1)	43.7	43.3
Octagonal	Monoclinic C2/c	(11-3)	2.93	2.93	θ(11-3/311)	88.0	88.3
		(311)	2.93	2.90	θ(11-3/42-2)	43.9	44.1
		(42-2)	2.04	2.01	θ(42-2/311)	43.7	44.1
Hexagonal	Tetragonal I41/a	(104)	6.27	6.25	θ(104/214)	30.1	29.9
		(214)	3.76	3.72	θ(214/110)	30.6	31.8
		(110)	6.64	6.58	θ(110/104)	61.1	61.8

Table S1. Electron diffraction analysis of KFCT crystals. By measuring distances and angles between diffraction spots it was possible to assign crystals with rectangular and octagonal shapes to the monoclinic polymorph and crystals with a hexagonal shape to the tetragonal polymorph.

	CPG-362	CPG-48	CPG-8
Surface area before crystallization (m^2/g)	4.8 ± 0.1	65 ± 1	164 ± 3
Surface area after crystallization (m^2/g)	4.5 ± 0.1	28 ± 1	34 ± 2

Table S2.

BET surface area analysis carried out before and after crystallization in different CPG particles demonstrating showing infiltration of the crystals. CPG-48 and CPG-8 surface areas drastically decreased after crystallization. The CPG-362 did not show large changes before and after crystallization due to the low surface area of these particles.

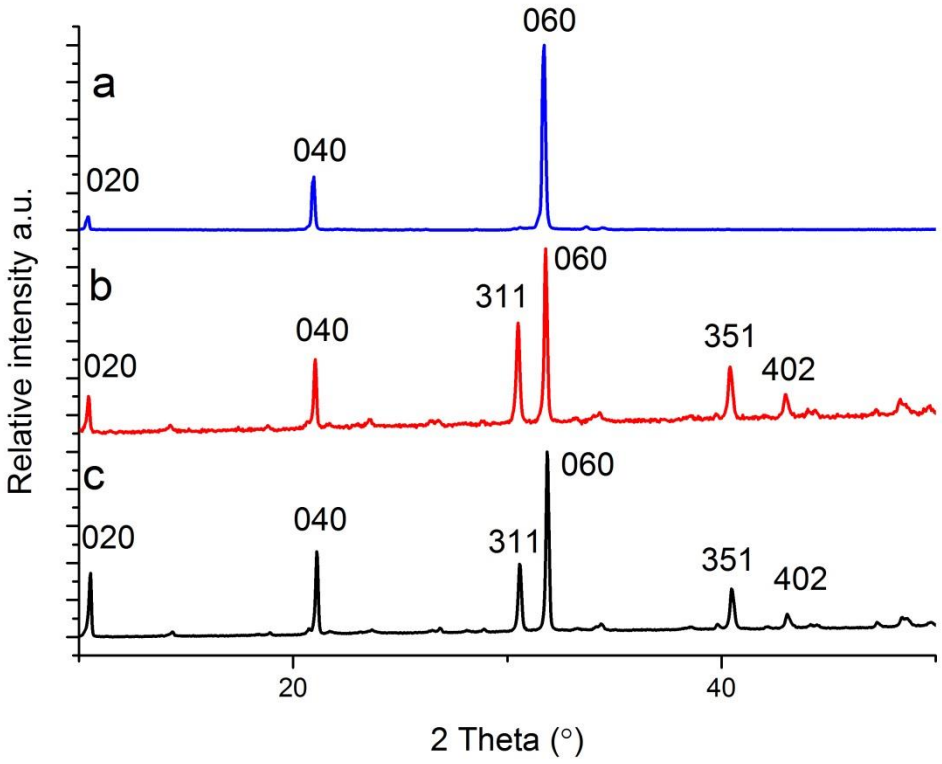

Figure S1. PXRD patterns of (a) large rectangular crystals (monoclinic) precipitated by evaporation in air under ambient conditions. These show a high degree of orientation along (010) reflections due to their plate-like shape; (b) the same crystals as (a) after grinding and (c) crystals precipitated by evaporation after 3 min, where these are a mixture of hexagonal-shaped (tetragonal) and rectangular crystals (monoclinic).

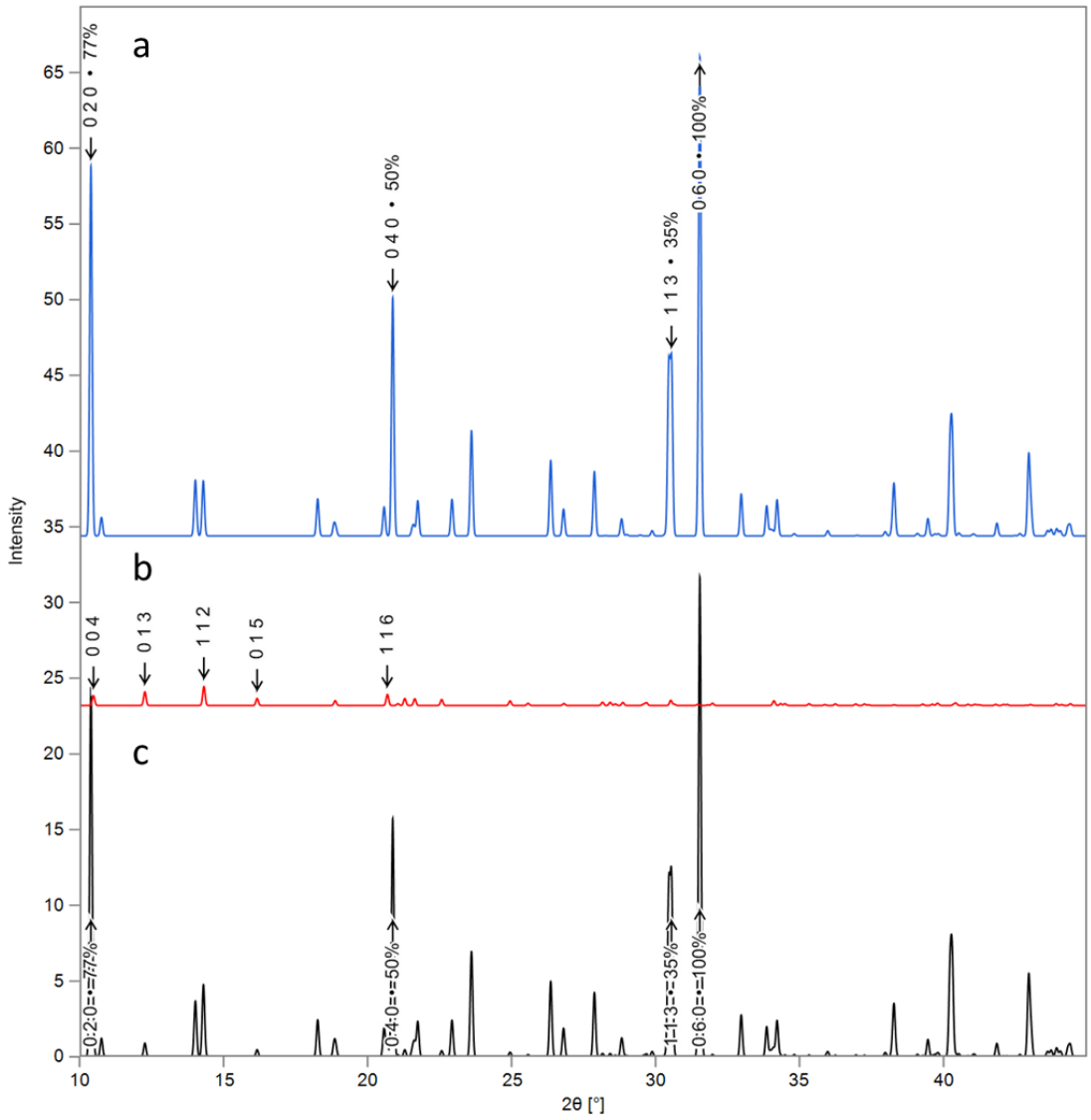

Figure S2. Calculated PXRD patterns using CrystalMaker software of (a) pure monoclinic KFCT and (b) pure tetragonal KFCT, and (c) mixture (5:5) of the two polymorphs based on the reference lattice parameters in Table 1. Only strong reflections are observed in the experimental diffraction patterns which mostly overlap for both polymorphs, making it hard to differentiate them in a sample containing a mixture of both phases.

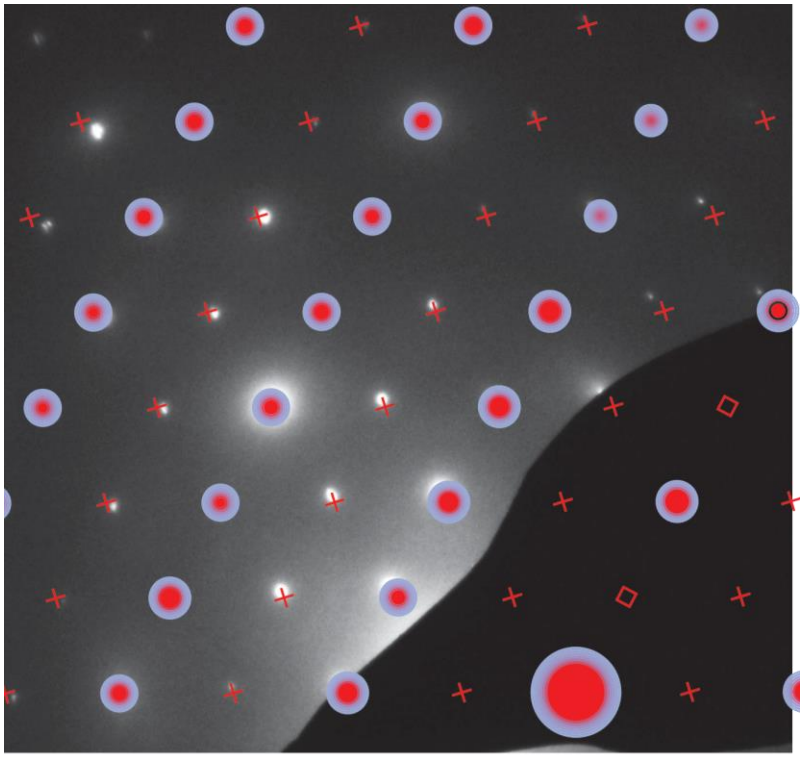

Figure S3. Corresponding simulated pattern with the observed diffraction pattern of a tetragonal crystal shown in figure 6f created using lattice parameters of a = 3.92, c = 33.72 $\alpha=\beta=\gamma=90$ zone axis [-4 4 1] using SingleCrystal software. Forbidden reflections are represented with x and ◊.

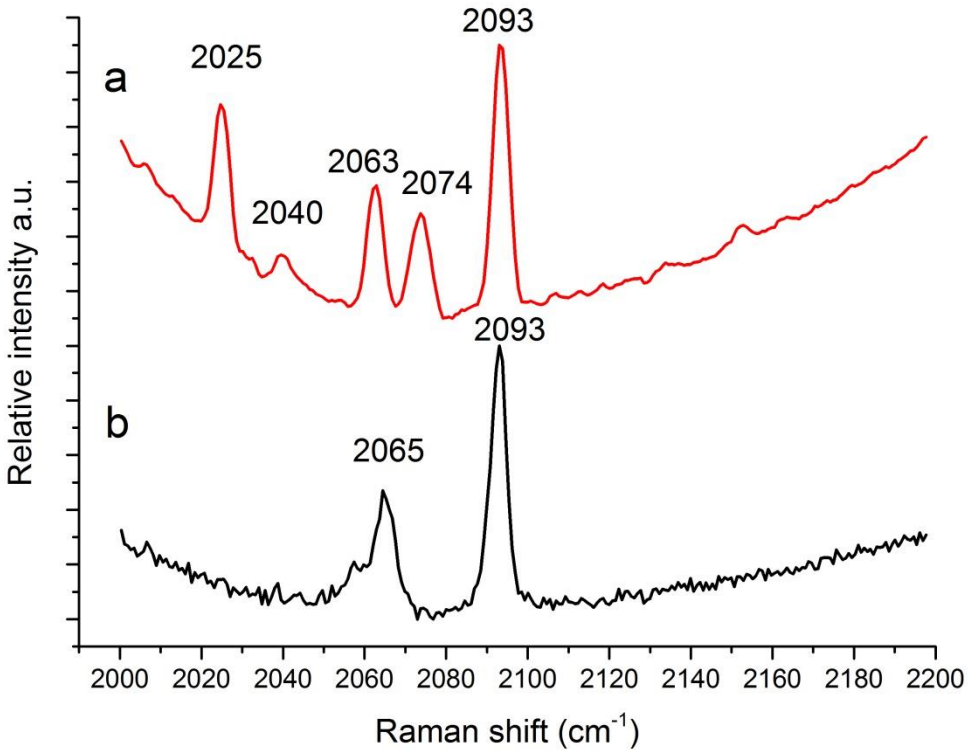

Figure S4. Raman spectra demonstrating the effect of humidity on the stability of the tetragonal crystals of KFCT precipitated in bulk solution, (a) after isolation, (b) after incubating in 100 % humidity when they had converted to the monoclinic polymorph within 15 min.

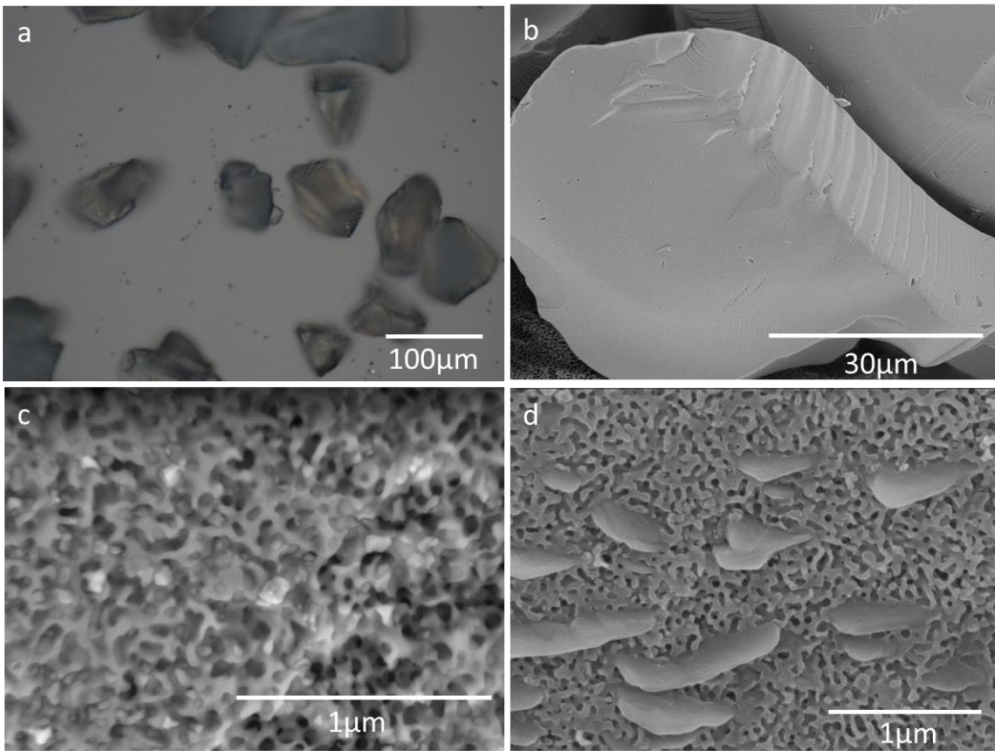

Figure S5. SEM images of CPG-48 particles after precipitation showing the absence of large crystals on the surface or in between particles (a,b) and higher magnification images of the CPG particles showing, (c) pores full of crystals and, (d) crystals of about 1 µm in length emerging from the pores.

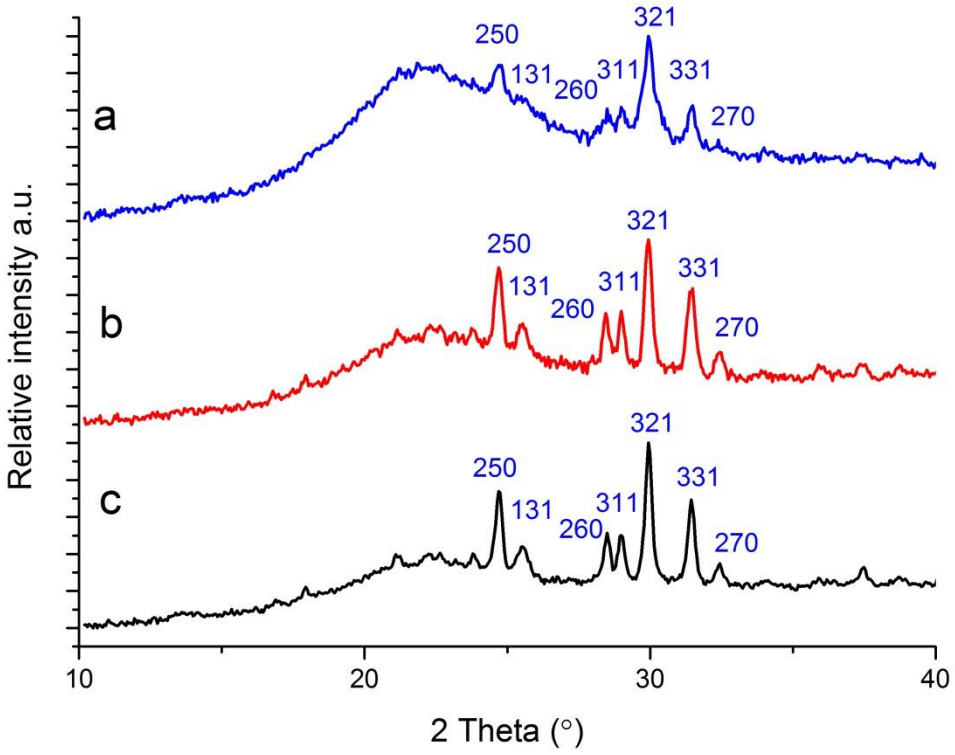

Figure S6. PXRD of crystals in CPGs after vacuum drying for 5h and exposure to ambient conditions for 1 month in CPG-362 (a), CPG-48 (b) and CPG-8 (c). All samples contain KFC crystals and ransformation to KFCT was not observed after one year of storage.

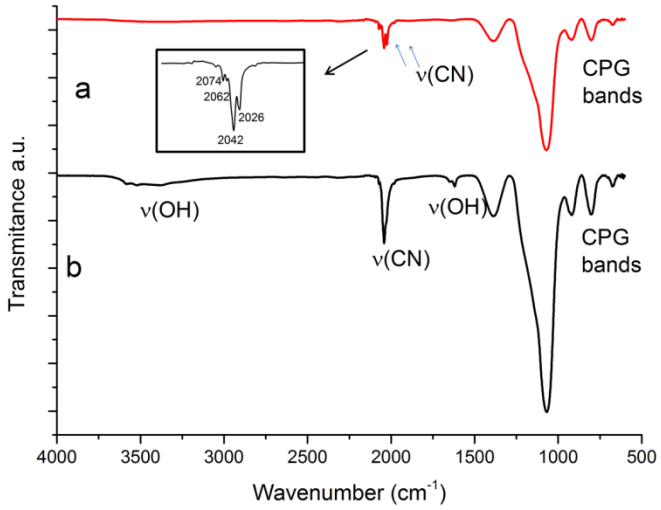

Figure S7. IR spectra of KFCT crystals precipitated within CPG-48; (a) vacuum-dried and maintained under ambient conditions for 1 month, showing the characteristic peaks of anhydrous KFC at 2072, 2061, 2037 and 2024 cm^{-1} and no peaks from hydrated KFCT, (b) Air-dried after 1 month, when KFCT peaks were observed at ≈ 3500 and 1647 and 1614 cm^{-1}. These derive from O-H stretching of the water molecules, while the 2037 cm^{-1} originates from the C≡N group. Note that the same results were obtained with all three pore sizes.

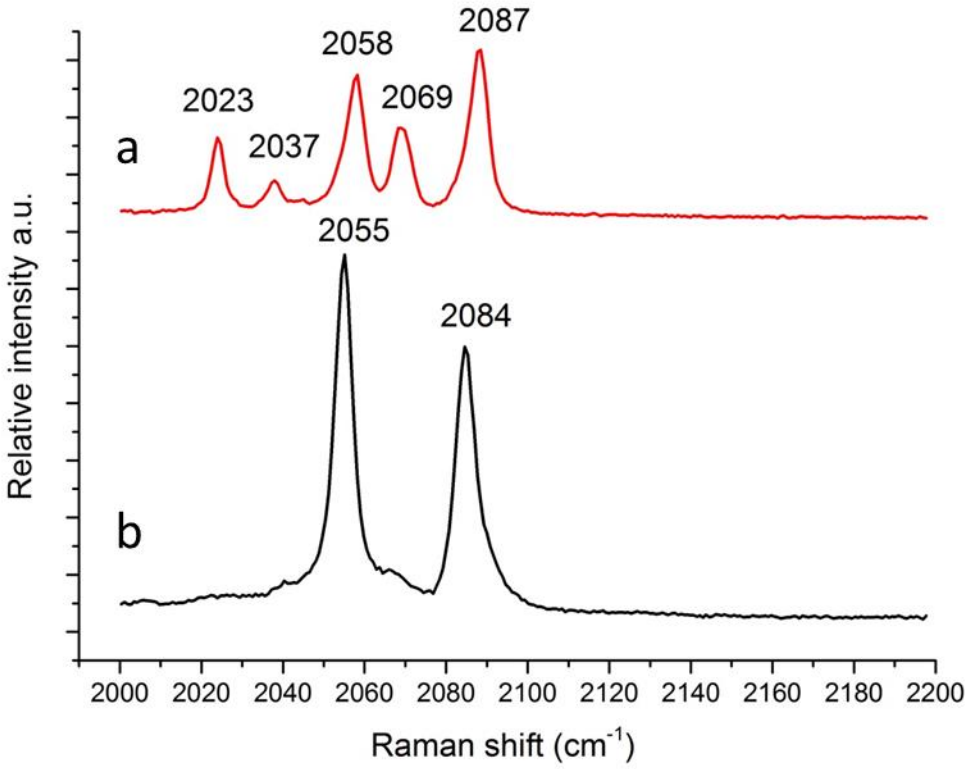

Figure S8. Raman spectra of CPG-48 after (a) vacuum drying and exposure to ambient conditions for 1 month. Peaks corresponding to anhydrous KFC are seen and no hydrated KFCT was observed. (b) After air-drying and exposre to ambient conditions for 1 month. Peaks corresponding to KFCT (mainly monoclinic) are seen. Note that the same results were obtained with all three pore sizes.

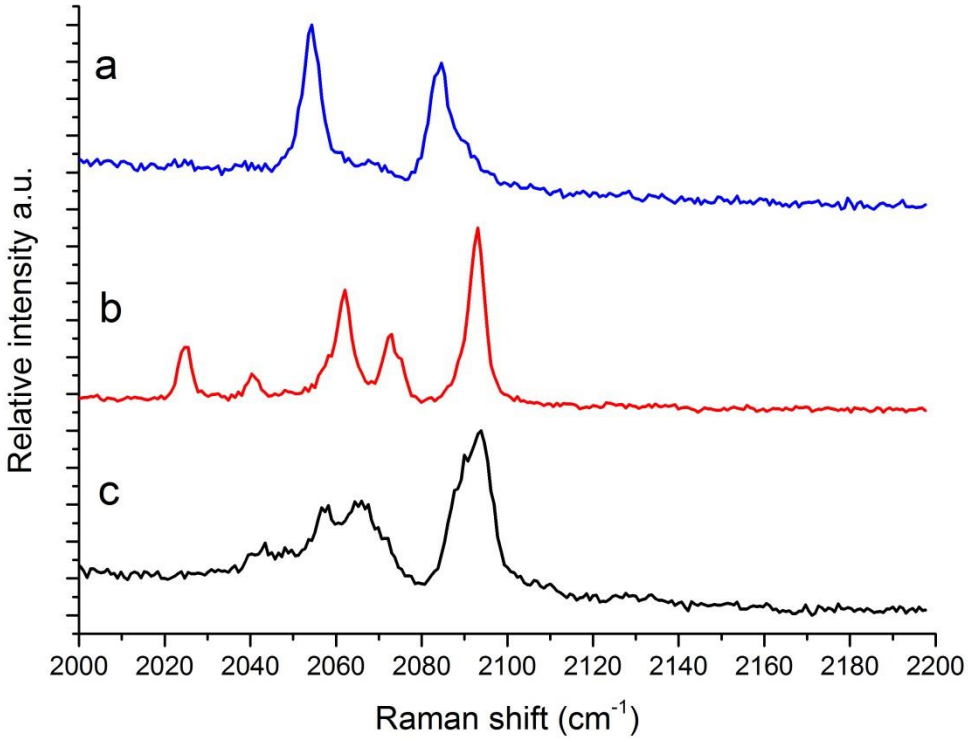

Figure S9. Raman analysis of KFCT crystals in CPG-48 after 2 days of evaporation where a mixture of polymorphs was found. 70% of the particles showed peaks at 2064 cm^{-1} and 2093 cm^{-1} only, corresponding to the monoclinic polymorph (a) while 30% of the particles showed peaks at 2024 cm^{-1}, 2040 cm^{-1}, 2064 cm^{-1}, 2093 cm^{-1} and 2071 cm^{-1} corresponding to the tetragonal polymorph (b). Particles with overlapping peaks were not included in the percentages (c).

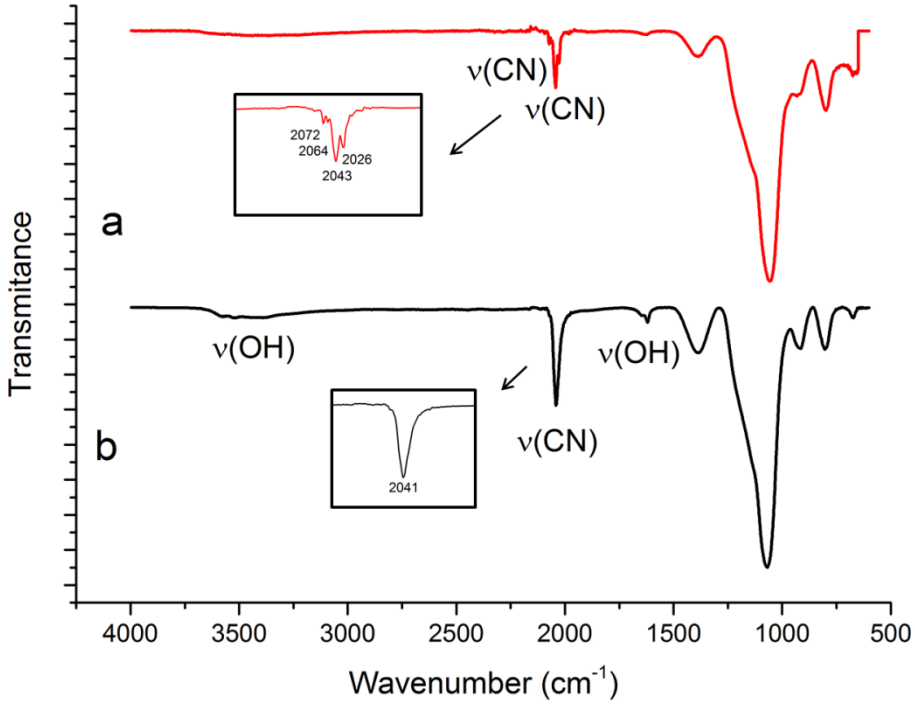

Figure S10. IR spectra of (a) vacuum-dried CPG-48/KFC with peaks from KFC at 2072, 2061, 2037 and 2024 cm^{-1} and (b) after incubation in 100% humidity for 2 days. The O-H stretching peak is at 1614 cm^{-1} and the peaks at 2072, 2061 and 2024 cm^{-1} are much reduced in intensity.

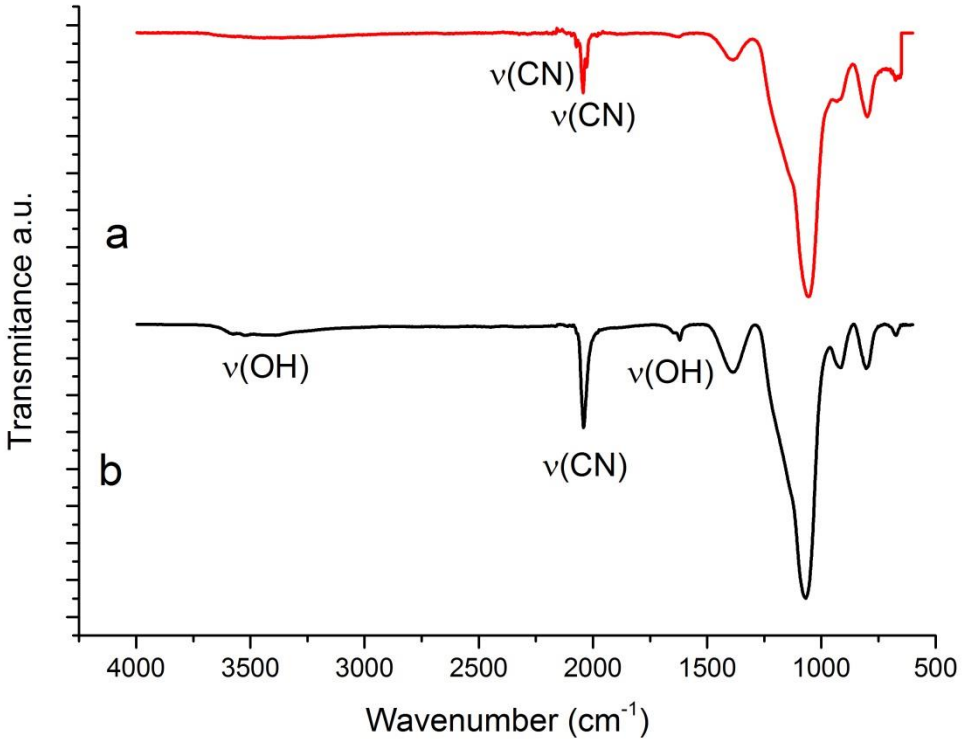

Figure S11. IR spectra of vacuum-dried CPG-8/KFC, (a) after incubation in ~100% humidity for 2 days. The water bands are not yet present and multiple peaks around 2000-2100 cm^{-1} are observed, (b) after incubation in 100% humidity for 2 weeks. Peaks from O-H bonds are evident at around 1600 cm^{-1} and the peaks at 2072, 2061 and 2024 cm^{-1} are much reduced in intensity.

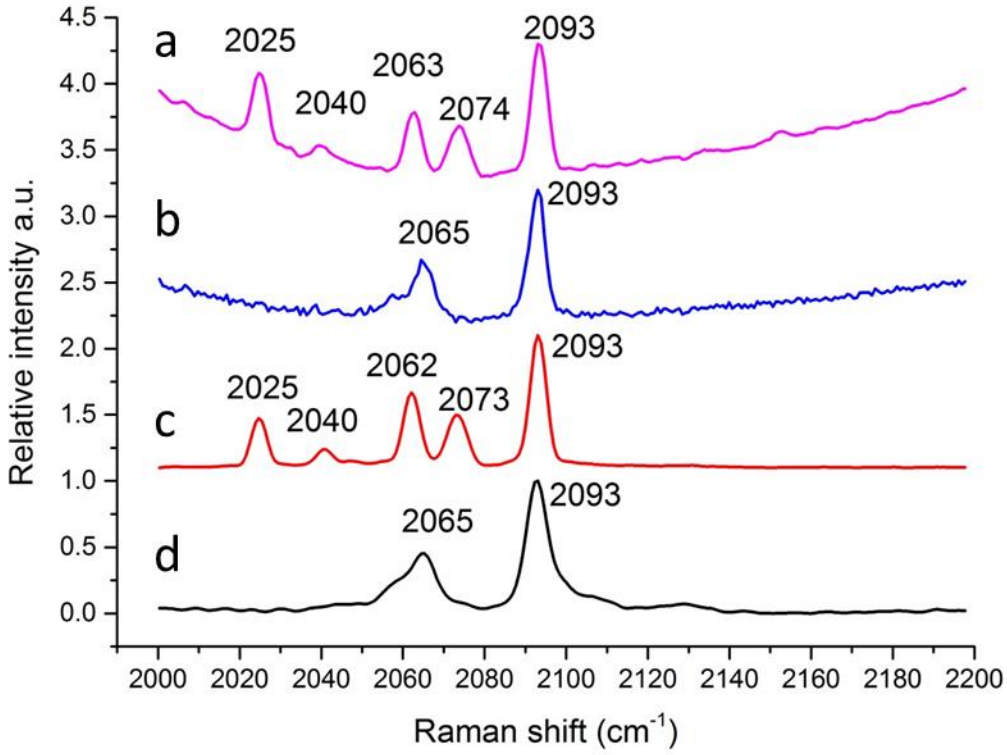

Figure S12. Raman spectra showing the effect of humidity on the stability of the tetragonal polymorph of KFCT in bulk solution (a, b) and in CPG-8 (c, d). (a) Tetragonal crystals were isolated in bulk, (b) after incubation in 100 % humid conditions they converted to the monoclinic polymorph in 15 min, (c) air-dried CPG-8 containing tetragonal crystals after 2 days, (d) after incubating sample (c) in 100% humid conditions conversion to the monoclinic polymorph occrred in 1h.